LA-UR-18-20539 (Accepted Manuscript)

Validation of statistical uncertainties in subcritical benchmark measurements: Part I – Theory and simulations

Hutchinson, Jesson D.
Nelson, Mark Andrew
Grove, Travis Justin
Arthur, Jennifer Ann
Cutler, Theresa Elizabeth
Bahran, Rian Mustafa
McKenzie, George Espy IV

Provided by the author(s) and the Los Alamos National Laboratory (2019-02-05).

To be published in: Annals of Nuclear Energy

DOI to publisher's version: 10.1016/j.anucene.2018.10.022

Permalink to record: http://permalink.lanl.gov/object/view?what=info:lanl-repo/lareport/LA-UR-18-20539

Disclaimer:
Approved for public release. Los Alamos National Laboratory, an affirmative action/equal opportunity employer, is operated by the Los Alamos National Security, LLC for the National Nuclear Security Administration of the U.S. Department of Energy under contract DE-AC52-06NA25396. Los Alamos National Laboratory strongly supports academic freedom and a researcher's right to publish; as an institution, however, the Laboratory does not endorse the viewpoint of a publication or guarantee its technical correctness.

Validation of Statistical Uncertainties in Subcritical Benchmark Measurements: Part I - Theory and Simulations

Jesson Hutchinson[a], Mark Nelson[a], Travis Grove[a], Jennifer Arthur[a,b], George McKenzie[a], Rian Bahran[a], Theresa Cutler[a]

[a] *Los Alamos National Laboratory, Los Alamos, NM 87545*
[b] *University of Michigan Department of Nuclear Engineering and Radiological Sciences, Ann Arbor, MI 48109*

Abstract

Subcritical neutron noise measurements are often used to determine multiplication of a system with Special Nuclear Material. This work presents an uncertainty approach which incorporates the singles and doubles counting rates determined by the Hage-Cifarelli formalism. This is a moments-based approach which utilizes time correlations between prompt neutrons in order to assess the system multiplication. After the method is described, a validation is presented which utilizes simulated data generated using a 0-D point-kinetics Monte Carlo code.

Keywords: neutron multiplicity, Feynman Variance-to-Mean, subcritical measurements, neutron noise

1. Introduction

Neutron multiplication is useful parameter to quantify in Special Nuclear Material (SNM) systems, as it depends upon all of the parameters that affect criticality, which includes the type, enrichment, and quantity of the SNM being measured. When a fission occurs, multiple neutrons may be emitted at the time of scission, and are therefore correlated in time. This property can be utilized

*Corresponding author
Email address: `jesson@lanl.gov` (Jesson Hutchinson)

to help understand the system multiplication. The primary parameters determined in neutron-based subcritical measurements generally include the leakage multiplication M_L or total multiplication M_T. These types of measurements have been performed since the 1940s and improvements in nuclear detection instrumentation and SNM availability in the 1950s and 1960s led to increased research activity in both the theory and practice of multiplication and reactivity measurements.

The *International Criticality Safety Benchmark Evaluation Project* (ICSBEP) Handbook [1] contains thousands of critical configurations. These evaluations include an evaluation of all systematic uncertainties in an experiment and undergoes extensive peer review. The ICSBEP handbook also includes subcritical configurations, but few such benchmarks currently exist. Recently three experiments with a 4.5 kg alpha-phase weapons grade plutonium sphere (BeRP ball) surrounded by copper [2], tungsten [3], and nickel [4] were performed. The nickel and tungsten benchmarks have been accepted by the ICSBEP. These evaluations are analyzed using the Hage-Cifarelli formalism based on the Feynman Variance-to-Mean method [5], and are the result of many years of collaborative subcritical experiment research [3, 4, 6, 7, 8, 9, 10, 11, 12, 13, 14, 15, 16]. This evaluation is classified as a fundamental physics benchmark, which focuses on quantifying singles counting rate (R_1), doubles counting rate (R_2), and leakage multiplication (M_L) instead of k_{eff} like critical benchmark evaluations; these three parameters will be discussed in detail in Section 2. This work expands upon methods which have previously been described [17, 18, 19] while improving upon the validation of statistical uncertainties. Part II of this work will apply the same approach to recently measured subcritical benchmark data.

2. Method

Prompt neutrons are produced from fission immediately after a fission event and are therefore correlated in time. Time information about detected neutron events can be used to determine characteristics of the system being measured.

Many different time-correlated methods have been used since the 1950s and are still widely utilized today [20, 21]. All time-domain neutron noise methods involve binning the measured data (or data derived from the measured data) into time gates. This work describes an uncertainty analysis applied to measured or simulated data using the Hage-Cifarelli formalism [5] of the Feynman Variance-to-Mean method [22]. Historically, correlated neutron measurements were made by using sophisticated time gating electronics to record counts observed within specific time intervals. However, since the 1990s, these types of measurements have generally been performed with detector systems that can record list-mode data which is a list of all times in which neutron counts were recorded in the detector system. Utilizing list-mode data allows for one to analyze the data in a variety of ways and at multiple time intervals which will be utilized often in this work. A number of works have investigated statistical uncertainties associated with the Feynman Variance-to-Mean method [23, 24, 25, 17, 19, 26, 18]. This work will utilize equations established in these publications and discuss differences between the methods. The focus of this work will be based on calculating statistical uncertainties for the parameters of interest, but a brief discussion on systematic uncertainties is also given.

2.1. Feynman histograms

In order to use the Feynman Variance-to-Mean method, the data must be binned. There are multiple binning methods which can be used to create Feynman histograms [27]; this study from 2014 concluded that both the random and sequential binning methods yielded similar (and accurate) results, especially for high count rate systems like those presented in this work. For this work, the sequential binning method was used which is shown in Figure 1. This binning method starts at a time of 0 and tallies the number of recorded events in each time interval (also referred to as gate or gate-width) τ over the entire file. The reason that the sequential (and not random) binning method is used for this work is because it is reproducible (the same results should be produced from the same file each time). After the data are binned, they can be displayed (for a

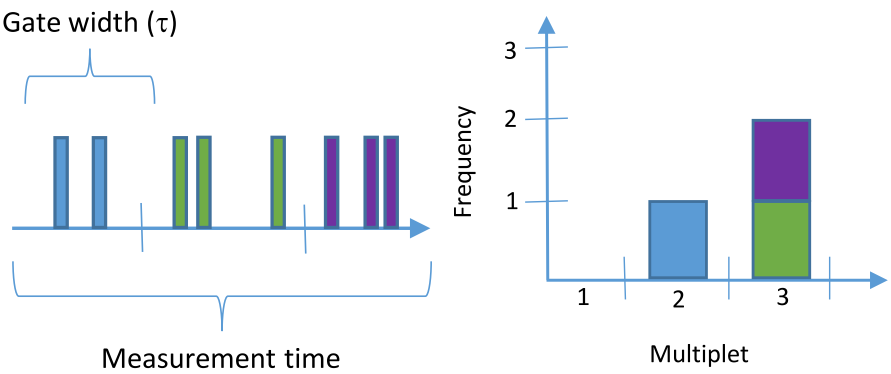

Figure 1: Sequential binning to create Feynman histograms

given gate-width τ) as a Feynman histogram. The histogram has two columns of data; one column is the number of neutrons recorded in a gate (known as n) and the other column is the number of gates that contained exactly n events (known as C_n), as shown in Figure 1. The sum of the total number of time bins is referred to as N. The total counting time is equal to τN and the normalized fraction of gates is shown in Equation 1.

$$p_n = \frac{C_n}{\sum_{n=0}^{\infty} C_n} = \frac{C_n}{N} \tag{1}$$

2.2. Moments of the counting distribution

The assumptions from the Hage-Cifarelli formalism [5] apply to this work; these include:

1. Point source assumption,
2. Fast neutron multiplication is taking place in the SNM,
3. No neutrons return from the detector to the SNM,
4. Induced fissions occur at the same time as the primary neutron emissions,
5. The time response of the moderator detector assembly is a pure exponential function,
6. The primary neutron energy has no influence on the thermal neutron detection probability,

7. There are no signal losses due to dead time,
8. There are no neutron chain restarts resulting from neutrons being reflected back from the moderator,
9. The SNM assembly is emitting a neutron flux which if observed in a large time gate (> 1 sec) is constant.

More complex models can be created to ensure the data are precisely described, but they run the risk of having too many variables that need to be adjusted. The general form for the reduced factorial moments is given in Equation 2. From this equation, one can show that the first four reduced factorial moments for any gate width are given by Equations 3-6.

$$m_r = \frac{\sum_{n=0}^{\infty} n\left(n-1\right)\dots\left(n-r+1\right)p_n}{r!} \tag{2}$$

$$m_1 = \sum_{n=0}^{\infty} np_n \tag{3}$$

$$m_2 = \frac{\sum_{n=0}^{\infty} n\left(n-1\right)p_n}{2!} = \frac{1}{2}\left[\sum_{n=0}^{\infty} n^2p_n - \sum_{n=0}^{\infty} np_n\right] \tag{4}$$

$$\begin{aligned} m_3 &= \frac{\sum_{n=0}^{\infty} n\left(n-1\right)\left(n-2\right)p_n}{3!} \\ &= \frac{1}{6}\left[\sum_{n=0}^{\infty} n^3p_n - 3\sum_{n=0}^{\infty} n^2p_n + 2\sum_{n=0}^{\infty} np_n\right] \end{aligned} \tag{5}$$

$$\begin{aligned} m_4 &= \frac{\sum_{n=0}^{\infty} n\left(n-1\right)\left(n-2\right)\left(n-3\right)p_n}{4!} \\ &= \frac{1}{24}\left[\sum_{n=0}^{\infty} n^4p_n - 6\sum_{n=0}^{\infty} n^3p_n + 11\sum_{n=0}^{\infty} n^2p_n - 6\sum_{n=0}^{\infty} np_n\right] \end{aligned} \tag{6}$$

In order to determine the uncertainties in these moments, it is convenient to express Equations 2-6 as shown in Equations 7-11. These are the factorial moments (not reduced) of the histogram which are used in other Feynman Variance-to-Mean analysis methods [28]. Both $\bar{C}_1$(sometimes called simply $\bar{C}$) and m_1 are the average number of counts that are recorded within the time interval τ.

$$\bar{C}_r = \sum_{n=0}^{\infty} n^r p_n \tag{7}$$

$$\bar{C}_1 = \sum_{n=0}^{\infty} n p_n (\tau) = m_1 \tag{8}$$

$$\bar{C}_2 = \sum_{n=0}^{\infty} n^2 p_n (\tau) = 2m_2 + m_1 \tag{9}$$

$$\bar{C}_3 = \sum_{n=0}^{\infty} n^3 p_n = 6m_3 + 6m_2 + m_1 \tag{10}$$

$$\bar{C}_4 = \sum_{n=0}^{\infty} n^4 p_n = 24m_4 + 36m_3 + 14m_2 + m_1 \tag{11}$$

Using the definition of the unbiased equation for sample variance, shown in Equation 12, one can solve for the uncertainties of the reduced factorial moments (δm_r) as shown in Equation 13. The uncertainty in the first moment and second moments are given in Equations 14-15.

$$s^2 = \frac{1}{N-1} \sum_{i=1}^{N} (x_i - \bar{x})^2 \tag{12}$$

$$\delta m_r = \sqrt{\frac{\left(\sum_{i=1}^{N} \frac{n(n-1)\ldots(n-r+1)}{r!} - m_r\right)^2 p_n}{N-1}} \tag{13}$$

$$\delta m_1 = \sqrt{\frac{\left(\sum_{i=1}^{N} n - m_1\right)^2 p_n}{N-1}} = \sqrt{\frac{2m_2 + m_1 - m_1^2}{N-1}} \tag{14}$$

$$\delta m_2 = \sqrt{\frac{\left(\sum_{i=1}^{N} \frac{n(n-1)}{2} - m_2\right)^2 p_n}{N-1}} = \sqrt{\frac{6m_4 + 6m_3 + m_2 - m_2^2}{N-1}} \tag{15}$$

Similarly, one can use Equation 16, the sample covariance, to determine the covariance between m_1 and m_2 as shown in Equation 17. It should be noted that the unbiased estimates use $\frac{1}{N}$ and not $\frac{1}{N-1}$; the value of N used for these types of problems is sufficiently large such that these two terms are equivalent and either can be used.

$$\delta jk = \frac{1}{N-1} \sum_{i=1}^{N} (x_{ij} - \bar{x_j})(x_{ik} - \bar{x_k}) \tag{16}$$

$$\begin{aligned} \delta m_1 m_2 &= \frac{1}{N-1} \left(\sum_{i=1}^{N} n - m_1 \right) \left(\sum_{i=1}^{N} \frac{n(n-1)}{2} - m_2 \right) p_n \\ &= \frac{1}{N-1} (3m_3 + 2m_2 - m_2 m_1) \end{aligned} \tag{17}$$

2.3. Excess Variance

As the name implies, the Feynman Variance-to-Mean method compares the variance of the counting distribution to the mean using Equation 18.

$$Y = \frac{\bar{C_2} - \bar{C_1}^2}{\bar{C_1}} - 1 = \frac{2m_2 + m_1 - m_1^2}{m_1} - 1 \tag{18}$$

In the Hage-Cifarelli formalism, a recursive formula for the reduced factorial moments is introduced [5], as shown in Equation 19 with $m_0 = 1$.

$$m_\mu = \sum_{r=0}^{\mu-1} \frac{\mu - r}{\mu} m_r m^*_{(\mu-r)} \tag{19}$$

Often, the terms Y_μ are used, as defined in Equation 20. The first two terms are given in Equations 21-22. Higher-order terms have been solved for in previous works [19] but are not shown here.

$$Y_\mu = \frac{m^*_\mu}{\tau} \tag{20}$$

$$Y_1 = \frac{1}{\tau} m_1 \tag{21}$$

$$Y_2 = \frac{1}{\tau}\left(m_2 - \frac{1}{2}m_1^2\right) \tag{22}$$

Given Equations 18 and 22, one can relate the term Y_2 to Y as shown in Equation 23.

$$Y_2 = \frac{Y\bar{C}_1}{2\tau} \tag{23}$$

Two different approaches are used to determine the uncertainties associated with the excess variance terms. The first approach (called the sum of differences approach), simply applies Equation 12 to Equations 21-22, which results in Equations 24-25. The covariance between Y_1 and Y_2 can be determined in the same fashion as shown in Equation 26. This approach has been previously used to determine uncertainties in these parameters [17, 18, 24].

$$\delta Y_1 = \frac{1}{\tau}\delta m_1 = \frac{1}{\tau}\sqrt{\frac{2m_2 + m_1 - m_1^2}{N-1}} \tag{24}$$

$$\delta Y_2 = \frac{1}{\tau}\delta m_2 = \frac{1}{\tau}\sqrt{\frac{6m_4 + 6m_3 + m_2 - m_2^2}{N-1}} \tag{25}$$

$$\delta Y_1 Y_2 = \frac{\delta m_1 m_2}{\tau^2} \tag{26}$$

A second method uses the propagation of uncertainty for a function $f(a, b)$, shown in Equation 27. This is applied to the Y_μ results in Equations 28-29. This approach has also been used previously [19, 23]. It can be seen by comparing Equations 24 and 28 that both approaches yield the same uncertainty for Y_1. An equation for the covariance between Y_1 and Y_2 is not given here, but is discussed in detail in Section 3.4. Comparing Equations 25 and 29, however, shows that the uncertainties for Y_2 are different. An internal report previously compared the two methods and showed that for these parameters, the propagation of uncertainties approach should be used instead of the sum of differences method [19]. This work agrees with that conclusion and is further discussed in Section 3.2.2.

$$\delta_f^2 = \left(\frac{\partial f}{\partial a}\right)^2 \delta_a^2 + \left(\frac{\partial f}{\partial b}\right)^2 \delta_b^2 + 2\frac{\partial f}{\partial a}\frac{\partial f}{\partial b}\delta_{ab} \tag{27}$$

$$\delta Y_1 = \frac{1}{\tau}\delta m_1 = \frac{1}{\tau}\sqrt{\frac{2m_2 + m_1 - m_1^2}{N-1}} \tag{28}$$

$$\delta Y_2 = \frac{1}{\tau}\sqrt{\frac{1}{N-1}(6m_4 - 6m_3m_1 + 6m_3 - m_2^2 + 4m_2m_1^2 - 4m_2m_1 + m_2 - m_1^4 + m_1^3)} \tag{29}$$

2.4. Singles and doubles counting rates

Determination of the detector counting rates requires application of the ω_μ terms shown in Equations 30-32. The term λ is equal to the fundamental mode prompt neutron decay constant of the system (including the slowing-down of neutrons in the detector system moderator, if present) which is discussed further in Section 2.5. The detector counting rates are determined using the excess variance and prompt neutron decay constant, as shown in Equations 33-35. The singles counting rate R_1 is the count rate observed in the detection system. In addition to being derived from this equation, R_1 is also equal to the total number of counts during the measurement (m_1N) divided by the total counting time (τN). It can be seen that the N terms cancel out and this is indeed the same equation. The doubles counting rate R_2 is the rate at which two neutrons from a single fission chain are detected.

$$\omega_\mu = \sum_{r=0}^{\mu-1} \begin{pmatrix} \mu - 1 \\ r \end{pmatrix} (-1)^r \, \frac{1 - e^{-\lambda\tau r}}{\lambda\tau r} \tag{30}$$

$$\omega_1 = 1 \tag{31}$$

$$\omega_2 = 1 - \frac{1 - e^{-\lambda\tau}}{\lambda\tau} \tag{32}$$

$$R_\mu = \frac{Y_\mu}{\omega_\mu} \tag{33}$$

$$R_1 = Y_1 \tag{34}$$

$$R_2 = \frac{Y_2}{\omega_2} \tag{35}$$

Since R_1 is equal to Y_1, the uncertainties of both parameters are equivalent. For the doubles counting rate, however, the uncertainty in λ must also be taken into account. Applying Equation 27 to Equation 35 and assuming that Y_2 and λ are uncorrelated results in Equation 36. The uncertainty in λ will be discussed further in Section 2.5.

$$\delta R_2 = \sqrt{\frac{1}{\omega_2^2}\left[\delta Y_2^2 + \frac{R_2^2}{\lambda^2}\left(1 - \omega_2 - e^{-\lambda\tau}\right)^2 \delta\lambda^2\right]} \tag{36}$$

2.5. Prompt neutron decay constant

As discussed in Section 2.4, the term λ is equal the prompt neutron decay constant, including neutrons slowing down in the detector moderator (if present). This term is equivalent to α in the Rossi-α method [22, 29], but when the term α is used in literature, it has typically not included slowing down in moderator which is part of a detector system. The inverse of the prompt neutron decay constant is often called the lifetime or slowing-down time (and these terms are considered equivalent within this work). Two methods will be discussed in this work to determine λ. In the first method, Y_2 is first determined at several gate widths using Equation 22. Next, the data are fit to the curve $A\omega_2$ in which λ and A are determined. The second method to determine λ is to perform a typical Rossi-α analysis using Equation 37 [20]; here $p(t)$ is the probability of detecting a neutron in the time interval Δ and A and B are constants related to the uncorrelated and correlated neutron emission respectively. Using either the Y_2 data or the Rossi-α approach, a second lifetime can also be fit, which may result in a more accurate answer for some systems [30]. This is shown in

Equation 38 for Rossi-α and this type of fit will be utilized in Part II of this work.

$$p(t)\Delta = A\Delta + Be^{-\lambda t}\Delta \tag{37}$$

$$p(t)\Delta = A\Delta + B_1 e^{-\lambda_1 t}\Delta + B_2 e^{-\lambda_2 t}\Delta \tag{38}$$

The uncertainty in λ is not easy to quantify because the value obtained is highly dependent upon the approach used (Y_2 or Rossi-α), the number of lifetimes used in the fit (single, double, or triple lifetime fit), the binning used on the data, and the the time intervals on which the fit is performed. This will be the focus of future work and is discussed in additional detail in Section 3.2.1.

2.6. Uncertainty of leakage multiplication

Using the Hage-Cifarelli method [5], one can relate the detector observables (R_1 and R_2) to parameters of interest in an SNM system as shown in Equations 39-44. These parameters include the leakage multiplication (M_L), spontaneous fission rate (F_S), and (α, n) neutron emission rate (S_α). The SNM mass can be determined using the spontaneous fission and/or (α, n) emission rates [31]. The detector efficiency (ϵ) is defined as the number of neutrons detected divided by the number of neutrons emitted (including all sources such as spontaneous fission,(α, n), and induced fission) in the same time period.

$$R_1 = \epsilon \left(b_{11} F_S + b_{12} S_\alpha\right) \tag{39}$$

$$R_2 = \epsilon^2 \left(b_{21} F_S + b_{22} S_\alpha\right) \tag{40}$$

with

$$b_{11} = M_L \bar{\nu}_{S1} \tag{41}$$

$$b_{21} = M_L^2 \left(\bar{\nu}_{S2} + \frac{M_L - 1}{\bar{\nu}_{I1} - 1} \bar{\nu}_{S1} \bar{\nu}_{I2} \right) \tag{42}$$

$$b_{12} = M_L \tag{43}$$

$$b_{22} = M_L^2 \frac{M_L - 1}{\bar{\nu}_{I1} - 1} \bar{\nu}_{I2} \tag{44}$$

The terms $\bar{\nu}_n$ refer to the nth order reduced factorial moments of the P_ν distribution (the probability of emitting ν fast neutrons per fission). These are determined the same way as the detected reduced factorial moments from Equation 2; the only difference is that here ν is used instead of n and P_ν is used instead of p_n. This results in the first two reduced factorial moments in Equations 45-46. The I and S subscripts refer to induced and spontaneous fission respectively. These values have been previously measured for many isotopes of interest [32, 33, 34], and are assumed to be known parameters. In addition, the uncertainties for these nuclear data parameters are assumed to be zero because nuclear data uncertainties are not included in measurement or experimental uncertainties in benchmark evaluations. A recent work showed that the uncertainties due to these terms do not have a large effect on the overall uncertainties for most Pu systems [35]. These terms are discussed in additional detail in Section 3.1.

$$\bar{\nu}_1 = \sum_{\nu=0}^{\infty} \nu P_\nu \tag{45}$$

$$\bar{\nu}_2 = \frac{1}{2} \sum_{\nu=0}^{\infty} \nu \left(\nu - 1\right) P_\nu \tag{46}$$

For systems that consist of spontaneous fission starter neutrons only, one can assume that S_α is equal to 0. Since the focus of this validation document will include metal Pu only, this assumption will be made, which results in Equations 47-48.

$$R_1 = \epsilon M_L \bar{\nu}_{S1} F_S \tag{47}$$

$$R_2 = \epsilon^2 M_L^2 F_S \left(\bar{\nu}_{S2} + \frac{M_L - 1}{\bar{\nu}_{I1} - 1} \bar{\nu}_{S1} \bar{\nu}_{I2} \right) \tag{48}$$

One can input any one of the three unknowns in these equations (ϵ, M_L, or F_S) to determine the other two. In addition, higher-order terms could also be used, but that is not done in this work. It is assumed that the value and uncertainty of the detector efficiency is known for this work, and leakage multiplication and spontaneous fission rate will be determined using the singles and doubles count rates. There are multiple methods that can be used to determine the efficiency of the detector system; for this work, we assume that replacement measurements (with a ^{252}Cf or other neutron source) are performed. For these replacement measurements, it is assumed that M_L is equal to 1; plugging this into Equation 47 results in Equation 49. Using Equation 27 with the assumption that R_1 and F_S are uncorrelated results in an uncertainty shown in Equation 50. This is a good assumption because the spontaneous fission rate is determined from an independent measurement (often provided in the form of a source certificate from the source manufacturer). It has been shown that the uncertainty in the source strength for replacement measurements can be one of the main contributors to the overall uncertainty in leakage multiplication [36].

$$\epsilon = \frac{R_1}{\bar{\nu}_{S1} F_S} \tag{49}$$

$$\delta\epsilon = \epsilon \sqrt{\left(\frac{\delta R_1}{R_1}\right)^2 + \left(\frac{\delta F_S}{F_S}\right)^2} \tag{50}$$

In order to determine the uncertainty in leakage multiplication, it is useful to rearrange Equation 47 to solve for spontaneous fission rate as shown in Equation 51. This can then be plugged into Equation 48 which results in the quadratic equation shown in Equation 52. Solving this results in Equation 53 for leakage multiplication.

$$F_S = \frac{R_1}{\epsilon M_L \bar{\nu_{S1}}} \tag{51}$$

$$\begin{aligned}
0 &= a_1 M_L^2 + a_2 M_L + a_3 \\
a_1 &= \frac{\bar{\nu_{S1}}\bar{\nu_{I2}}}{\bar{\nu_{I1}} - 1} \\
a_2 &= \bar{\nu_{S2}} - \frac{\bar{\nu_{S1}}\bar{\nu_{I2}}}{\bar{\nu_{I1}} - 1} \\
a_3 &= -\frac{R_2 \bar{\nu_{S1}}}{R_1 \epsilon}
\end{aligned} \tag{52}$$

$$M_L = \frac{-a_2 + \sqrt{a_2^2 - 4a_1a_3}}{2a_1} = \frac{-a_2 + a_4}{2a_1} \tag{53}$$

$$a_4 = \sqrt{a_2^2 - 4a_1a_3} \tag{54}$$

Applying Equation 53 to Equation 27 results in the uncertainty in leakage multiplication shown in Equation 55. This assumes that the detector efficiency is not correlated with the singles and doubles count rates. This assumption is valid if the efficiency is determined from an independent measurement (such as the replace measurement described above). The partial derivatives are given in Equation 55. For this work, it is also assumed that the covariance between the singles and doubles count rates ($\delta R_1 R_2$) is equal to zero. This assumption is discussed further in Section 3.4.

$$\delta M_L = \sqrt{\left(\frac{\partial M_L}{\partial R_1}\right)^2 \delta R_1^2 + \left(\frac{\partial M_L}{\partial R_2}\right)^2 \delta R_2^2 + 2\frac{\partial M_L}{\partial R_1}\frac{\partial M_L}{\partial R_2}\delta R_1 R_2 + \left(\frac{\partial M_L}{\partial \epsilon}\right)^2 \delta\epsilon^2} \tag{55}$$

$$\begin{aligned}
\frac{\partial M_L}{\partial R_1} &= \frac{a_3}{R_1 a_4} \\
\frac{\partial M_L}{\partial R_2} &= -\frac{a_3}{R_2 a_4} \\
\frac{\partial M_L}{\partial \epsilon} &= \frac{a_3}{\epsilon a_4}
\end{aligned}$$

2.7. Uncertainty in spontaneous fission rate

Once the value and uncertainty of the leakage multiplication has been determined, one could use Equation 51 to solve for the spontaneous fission rate. One could then apply the same approach to solve for the uncertainty in F_S. Doing so, however, results in uncertainties that are unrealistically large since it includes contributions from M_L (and the uncertainty in leakage multiplication is dependent upon the spontaneous fission rate). A better approach is to start back at Equation 47 and rearrange to solve for the leakage multiplication as shown in Equation 56. Plugging this into Equation 48 results in Equation 57, another quadratic equation.

$$M_L = \frac{R_1}{\epsilon F_S \bar{\nu}_{S1}} \tag{56}$$

$$\begin{aligned} F_S &= \frac{a_5 + \sqrt{a_5^2 + 4R_2 a_6}}{2R_2} = \frac{a_5 + a_7}{2R_2} \\ a_5 &= -\frac{R_1^2 \left(\bar{\nu}_{I2}\bar{\nu}_{S1} + \bar{\nu}_{S2} - \bar{\nu}_{I1}\bar{\nu}_{S2}\right)}{\left(\bar{\nu}_{I1} - 1\right)\bar{\nu}_{S1}^2} \\ a_6 &= \frac{\bar{\nu}_{I2} R_1^3}{\left(\bar{\nu}_{I1} - 1\right)\bar{\nu}_{S1}^2 \epsilon} \\ a_7 &= \sqrt{a_5^2 + 4R_2 a_6} \end{aligned} \tag{57}$$

Applying Equation 57 to Equation 27 gives the uncertainty shown in Equation 58. Similar to the uncertainty in leakage multiplication, it is assumed that the covariance between the singles and doubles count rates ($\delta R_1 R_2$) is equal to zero.

$$\delta F_S = \sqrt{\left(\frac{\partial F_S}{\partial R_1}\right)^2 \delta R_1^2 + \left(\frac{\partial F_S}{\partial R_2}\right)^2 \delta R_2^2 + 2\frac{\partial F_S}{\partial R_1}\frac{\partial F_S}{\partial R_2}\delta R_1 R_2 + \left(\frac{\partial F_S}{\partial \epsilon}\right)^2 \delta\epsilon^2} \tag{58}$$

$$\frac{\partial F_S}{\partial R_1} = \frac{a_5 a_7 + a_5^2 + 3a_6 R_2}{R_1 R_2 a_7}$$
$$\frac{\partial F_S}{\partial R_2} = \frac{a_6}{R_2 a_7} - \frac{a_5 + a_7}{2R_2^2}$$
$$\frac{\partial F_S}{\partial \epsilon} = -\frac{a_6}{\epsilon a_7}$$

2.8. Systematic uncertainties

The sections above focused on determining the values and statistical uncertainties for parameters of interest. In addition, systematic uncertainties are also present. One way to handle systematic uncertainties is to use the same approach used for critical experiments in the ICSBEP handbook [1, 37]. Assessment of the systematic uncertainties could be determined using measurements, but generally perturbation simulations are used for this purpose (generally with a 3-D Monte Carlo code). In order to estimate the systematic uncertainties of the parameters of interest (such as R_1,R_2, and M_L), one must first determine the uncertainties associated with each experimental parameter. The experimental parameters are often grouped into four categories: mass, dimensions, position, and compositions. For subcritical benchmarks, a fifth category is also used which includes parameters related to the radiation detection system. Generally each of these categories have multiple experimental parameters (mass for instance may include uncertainties associated with masses of the SNM, cladding, and reflectors). Generally, somewhere between 10-50 experimental parameters (referred to as x_i in Equations 59 and 60) are evaluated. The uncertainty in each parameter must be determined for each measured configuration. This is determined using information from logbooks, chemical analyses, drawings, pictures, and standards. Next, perturbation simulations are performed to determine sensitivity coefficients (S_{p,x_i}) given in Equation 59. Here p is the parameter of interest (such as R_1, R_2, and M_L); it should be noted that for critical experiments, p is generally k_{eff}. The uncertainty in parameter p is simply determined by multiplying the sensitivity coefficient by the uncertainty in the parameter as shown in Equation 60. It should be noted that the terms $(x_p - x_{ref})$ and δx_i are not equivalent; the former refers to the change in the experimental parameter used in the perturbation study while the latter refers to the uncertainty in the experimental parameter.

$$S_{p,x_i} = \frac{p_p - p_{ref}}{x_p - x_{ref}} \tag{59}$$

$$\delta p_i = S_{p,x_i} \delta x_i \tag{60}$$

If the experimental parameters are uncorrelated, one can determine the overall uncertainty in the parameter of interest by performing a sum of squares. If the parameters are correlated, then the covariance between the parameters must be taken into account. Last, one can determine a combined uncertainty in a parameter by taking a sum of squares of the systematic and statistical uncertainties. Much more detail has been documented on this subject, particular for critical experiment k_{eff} benchmarks [37]. The treatment of systematic uncertainties is given in Section 2 of ICSBEP evaluations. The determination of systematic uncertainties is not included in the validation below as it is specific to individual experiments.

3. Validation

This section will introduce the cases which will be used for validation and then show the validation results.

3.1. Validation test cases and nuclear data

The validation test cases for this work were created using the LANL Neutron Generator software [38]. This software is a 0-D point-kinetics Monte Carlo code which produces list-mode data in the same format as several LANL detectors. Four test cases were generated for this work as shown in Table 1; this table includes all of the inputs used for the Neutron Generator software. These test cases were chosen to bound the multiplication, count rates, and lifetimes associated with typical Pu benchmark measurements. The lower multiplication

Table 1: Neutron Generator inputs for test cases.

Case #	1	2	3	4
^{240}Pu spontaneous fission rate (F_S)	130423 sf/s			
Total multiplication (M_T)	4.4	4.4	20.0	20.0
Leakage multiplication (M_L)	3.2	3.2	13.0	13.0
Detector efficiency (ϵ)	0.022 $\pm$0			
Dead time (μs)	0			
Lifetime ($\frac{1}{\lambda}$, μs)	40	200	40	200
Time per file (sec)	60		12	
Number of files	800			

value investigated (total multiplication, M_T , of 4.4) is that of the bare BeRP ball. The upper multiplication value examined was 20, which bounds the total multiplication for all current configurations in subcritical Pu benchmarks. The efficiency is that of a LANL detector used in a typical setup for benchmark measurements; the uncertainty of the efficiency will be zero for this work, since it is an input to the Neutron Generator software. Two lifetime values were examined that bounded all configurations in Pu subcritical benchmarks. The fast lifetime value of 40 μs is a typical value for LANL detector systems with polyethylene moderation [3, 4]. The slower lifetime value of 200 μs is bounding of any configurations in current Pu benchmarks. Each of the individual files has over 1 million events.

Information regarding the binning parameters used for the prompt neutron decay constant analysis is shown in Table 2. For the Feynman Variance-to-Mean method, the binning structure shown in Table 2 is generally used for Pu benchmarks. Cases 2 and 4, however, required the use of larger time intervals, since the lifetime is slower.

Case 1 is expected to give the best results, since it clearly meets all of the assumptions detailed in Section 2.2. Being slower systems, both Cases 2 and 4 could potentially violate assumptions 2 (fast neutron multiplication is taking

Table 2: Binning for prompt neutron decay constant analysis.

Method	Rossi-α	Feynman Variance-to-Mean (Y_2)	
Cases	1-4	1,3	2,4
Minimum time interval (μs)	5	4	16
Number of time intervals	1995	512	512
Maximum time interval (μs)	1999	2048	8192

Table 3: Reduced factorial moments of neutron emission from fission.

^{239}Pu		^{240}Pu	
$\bar{\nu_{I1}}$	3.182	$\bar{\nu_{S1}}$	2.154
$\bar{\nu_{I2}}$	4.098	$\bar{\nu_{S2}}$	1.894

place in the SNM) and 8 (there are no neutron chain restarts resulting from neutrons being reflected back from the moderator). When the multiplication and count rate are high (such as in Cases 3 and 4), the mean of the Feynman histogram occurs at large n. When this happens, a slight variation in C_n can greatly affect the higher-order moments. This leads to large variations in Y_2 at larger gate widths, which results in large uncertainties and further impacts the multiplication and spontaneous fission rate results.

As mentioned, the test cases represent a sphere of weapons-grade Pu and are bounding of the configurations used in previous subcritical benchmarks. The nuclear data reduced factorial moments for this work are given in Table 3. This work assumes that all spontaneous fission events occur in ^{240}Pu and all induced fission events occur in ^{239}Pu. To determine the average number of neutrons emitted, $\bar{\nu_{I1}}$, a simulation was used which produced weights that were applied to the ENDF/B-VII.1 data for fission in ^{239}Pu, as described in previous work [17, 18]. The second moment, $\bar{\nu_{I2}}$, was determined from the first moment using a data table which relates the first and second moments of the P_ν distribution for ^{239}Pu induced fission [33]. For spontaneous fission in ^{240}Pu, the data were taken directly from published work [34].

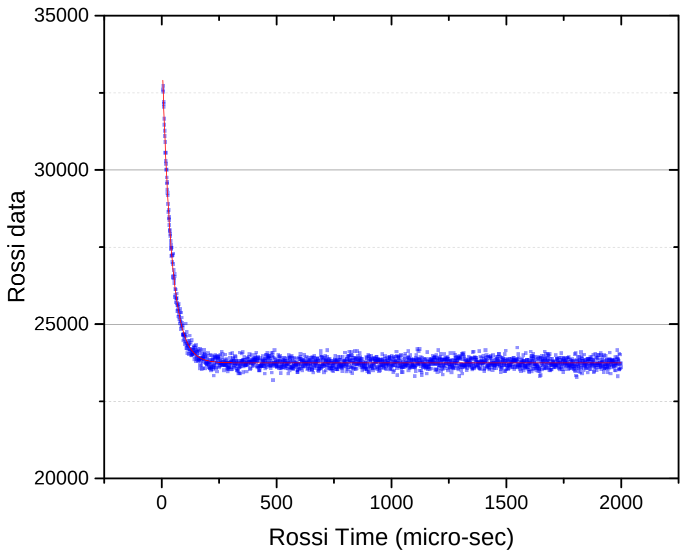

Figure 2: Rossi-α data for Case 1 (file 1 of 800).

3.2. Validation results

The results include a validation of singles count rate (R_1), Y_2, neutron lifetime ($\frac{1}{\lambda}$), doubles count rate (R_2), and leakage multiplication (M_L) values and uncertainties. In addition, there are subsections discussing the covariance between the singles and doubles count rate and selecting optimal time bins.

3.2.1. Neutron lifetime

Two methods were used to determine the prompt neutron decay constant (λ): the Rossi-α method and the Feynman Variance-to-Mean method (in which the Y_2 data are used to determine λ). An example of typical Rossi-α and Y_2 data (for a single file from Case 1) are shown in Figures 2 and 3, respectively.

In both methods, a fit of the data is performed to determine the prompt neutron decay constant (λ). It has been observed that a double lifetime fit often works better (even for bare systems) than a single lifetime fit using measured data [30]. This work uses simulated data, however, and a single exponential fit was judged to be appropriate for all four cases. Table 4 shows the results of performing these fits for 50 of the 800 data files for each case. This table shows

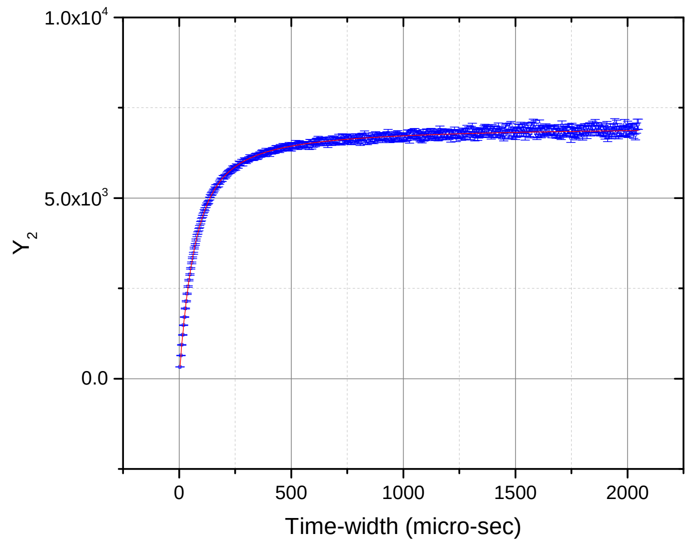

Figure 3: Y_2 data for Case 1 (file 1 of 800).

the neutron lifetime ($\frac{1}{\lambda}$), and as discussed in Section 2.5, this lifetime includes slowing down in the detector system (if a moderator is present in the detector system). It should be noted from this table that the average uncertainty reported in the fit is not equal to (and generally underestimates) the standard deviation (σ) associated with the lifetime for the 50 files. This is simply the uncertainty in the fit, not the uncertainty in the parameter. One cannot, however, use the standard deviation of these fits as the uncertainty in the lifetime either. This is because significantly different values could be obtained if one were to modify the way in which the data were fit; this includes the number of lifetimes used in the fit (single, double, or triple lifetime fit), the binning used on the data, and the time intervals on which the fit is performed. As an example, for the Rossi-α method, the results shown here used all of the data from 5-2000 μs; if the fit went out even further one could potentially get a better χ^2value, even though the fit is starting to include more and more of the uncorrelated portion of the graph.

This work uses a bounding approach. Here, the difference between the max and min of the neutron lifetime for the 50 files is determined and (after rounding

Table 4: Neutron lifetime (μs) values and standard deviation from fits of 50 data files for each case.

Method	Rossi-α			Y_2		
Time interval (τ)	Average	σ	Max-Min	Average	σ	Max-Min
Case 1	40.1	0.5	2.0	40.0	0.7	3.1
Case 2	200.6	5.4	27.2	199.6	7.6	32.7
Case 3	40.5	0.4	1.5	39.4	0.6	2.8
Case 4	200.1	3.4	12.9	189.0	4.9	21.8

up), it is assumed to be bounding of all possible values. The uncertainty in the lifetime is therefore taken to be that given in Equation 61 [37]. The assumed bounding time was 10 μs for Cases 1 and 3 and 40 μs for Cases 2 and 4; this results in $\delta(\frac{1}{\lambda})$ values of 2.89 and 11.55 μs respectively. As will be seen in the additional results section, this does result in doubles count rate (R_2) and leakage multiplication (M_L) which are slightly conservative. This approach is not necessarily the best approach available and will be the focus of future work.

$$\delta(\frac{1}{\lambda}) = \frac{bounding}{2\sqrt{3}} \tag{61}$$

3.2.2. Singles count rate (R_1), doubles count rate (R_2), leakage multiplication (M_L), and spontaneous fission rate (F_S)

The approach described in Section 2 was applied to each of the 800 files for each of the four cases, shown in Tables 5-8. This was performed at three different time intervals (τ): 512, 1024, and 2048 μs. The appropriate selection of a time gate will be discussed further in Section 3.3. It should be noted, as shown in Equation 34, that R_1 is equal to Y_1. It can be seen in Table 5 that for Case 1 the standard deviation of the 800 files compare very well to the average uncertainties determined from Equations 28 (for δR_1), 29 (for δY_2), 36 (for δR_2), 55 (for δM_L), and 58 (for δF_S). This excellent comparison helps provide confidence that the propagation of uncertainty method proposed is valid. It should be noted that the sum of differences method for the uncertainty in Y_2

Table 5: Singles count rate (R_1), Y_2, doubles count rate (R_2), leakage multiplication (M_L), and spontaneous fission rate (F_S) for Case 1.

		Time interval (τ)		
Parameter		512	1024	2048
Singles count rate (R_1)	Value	19884	19884	19884
	Uncertainty	23	23	24
	Standard deviation	24	24	24
Y_2	Value	6339	6610	6738
	Uncertainty	73	101	141
	Standard deviation	73	100	140
Doubles count rate (R_2)	Value	6877	6879	6872
	Uncertainty	90	107	144
	Standard deviation	79	104	143
Leakage Multiplication (M_L)	Value	3.17	3.17	3.17
	Uncertainty	0.02	0.02	0.03
	Standard deviation	0.02	0.02	0.03
Spontaneous fission rate (F_S)	Value	132323	132305	132373
	Uncertainty	817	961	1280
	Standard deviation	669	895	1239

(given in Equation 25) was shown not to be valid. For example, at a 2048 μs interval, the uncertainty in Y_2 for Case 1 was 988; this is 7 times higher than the standard deviation in Y_2 among the 800 files. This very large over prediction was seen in all of the results; they are therefore not further reported in this work.

Table 6 shows that for the slower Case 2, the uncertainties given by the proposed method also agreed quite well with the standard deviation in the data for all of the parameters. It can be seen, however, that the uncertainty method is quite a bit larger than the standard deviation results for R_2 and M_L at the smallest time interval (512 μs). This is likely due to the uncertainty in neutron

Table 6: Singles count rate (R_1), Y_2, doubles count rate (R_2), leakage multiplication (M_L), and spontaneous fission rate (F_S) for Case 2.

		Time interval (τ)		
Parameter		512	1024	2048
Singles count rate (R_1)	Value	19885	19885	19885
	Uncertainty	23	23	23
	Standard deviation	24	24	24
Y_2	Value	4400	5547	6212
	Uncertainty	66	94	136
	Standard deviation	67	97	139
Doubles count rate (R_2)	Value	6882	6884	6884
	Uncertainty	206	149	157
	Standard deviation	105	120	154
Leakage Multiplication (M_L)	Value	3.17	3.17	3.17
	Uncertainty	0.04	0.03	0.03
	Standard deviation	0.02	0.02	0.03
Spontaneous fission rate (F_S)	Value	132281	132281	132285
	Uncertainty	1318	1318	1388
	Standard deviation	1032	1032	1331

lifetime, which is conservatively estimated as described in the previous section. An overestimation in this uncertainty will affect the results most at smaller time intervals (due to the derivative of the ω_2 parameter).

Table 7 shows that there are much larger differences between the uncertainties given by the proposed method and the standard deviation of the data for Case 3. This is especially true for the larger time intervals (1024 and 2048 μs). This is at least partially due to the large uncertainties in the higher-order moments for these systems that have both very high multiplication and counting rates. When comparing Tables 5 and 7, it can be seen that while the singles count rate increased by a factor of about 4, the doubles count rate increased by

Table 7: Singles count rate (R_1), Y_2, doubles count rate (R_2), leakage multiplication (M_L), and spontaneous fission rate (F_S) for Case 3.

		Time interval (τ)		
Parameter		512	1024	2048
Singles count rate (R_1)	Value	82689	82671	82644
	Uncertainty	351	311	311
	Standard deviation	337	343	344
Y_2	Value	515890	535754	542827
	Uncertainty	9935	10234	12391
	Standard deviation	9519	12019	15109
Doubles count rate (R_2)	Value	559535	557497	553623
	Uncertainty	11355	10775	12663
	Standard deviation	10324	12507	15409
Leakage Multiplication (M_L)	Value	13.07	13.04	13.00
	Uncertainty	0.13	0.13	0.15
	Standard deviation	0.10	0.13	0.16
Spontaneous fission rate (F_S)	Value	133560	133762	134168
	Uncertainty	1573	1471	1679
	Standard deviation	901	1150	1539

a factor of 88. These incredibly high count rates are close to the boundary of what many ^{3}He-based detector systems can tolerate before saturation.

The results of Case 4, as expected, are the worst of all cases as shown in Table 8. This is because it combines the challenging qualities of a slower system (like Case 2 in Table 6) with a high multiplication and count rate (like Case 3 in Table 7). This type of configuration may violate some of the initial assumptions which were described in Section 2.2.

Another way to view the uncertainty results is to bin the results for the parameters of interest for each of the 800 files. This is shown in Figure 4 for Case 1 with a time interval of 1024 μs. These figures show the average results

Table 8: Singles count rate (R_1), Y_2, doubles count rate (R_2), leakage multiplication (M_L), and spontaneous fission rate (F_S) for Case 4.

		Time interval (τ)		
Parameter		512	1024	2048
Singles count rate (R_1)	Value	82735	82714	82679
	Uncertainty	215	280	290
	Standard deviation	318	319	323
Y_2	Value	359434	450967	500876
	Uncertainty	4951	8473	11174
	Standard deviation	6775	9765	13548
Doubles count rate (R_2)	Value	555205	556054	553444
	Uncertainty	16410	12894	12858
	Standard deviation	10464	12040	14970
Leakage Multiplication (M_L)	Value	13.01	13.02	13.00
	Uncertainty	0.19	0.15	0.15
	Standard deviation	0.11	0.13	0.16
Spontaneous fission rate (F_S)	Value	134181	134035	134272
	Uncertainty	2015	1665	1680
	Standard deviation	976	1186	1555

of each parameter in addition to the uncertainty and standard deviation results. Similar to the tables previously discussed, the uncertainties ("unc" in the figure) were determined from Equations 28 (for δR_1), 29 (for δY_2), 36 (for δR_2), 55 (for δM_L), and 58 (for δF_S) and are the average of the uncertainties calculated for each of the 800 files. This should be compared to the standard deviation ("sd" in the figures) of the 800 files. It can be seen that there is excellent agreement between the uncertainty and standard deviation for R_1 and Y_2 in Figures 4. The uncertainties are slightly larger than the standard deviations for R_2 and M_L in Figures 4, which is likely due to the conservative estimate on the neutron lifetime as discussed in Section 3.2.1.

Ideally, both the standard deviation of the 800 files and the average of the uncertainties for the 800 files would obey the 68-95-99.7 rule. Given that these are roughly Gaussian distributions, it is expected that 68% of the data are within ± 1 standard deviation of the mean, 95% of the data are within ± 2 standard deviations of the mean, and 99.7% of the data are within ± 3 standard deviations of the mean. Figure 5 shows the percentage of data which falls within 1, 2, and 3 standard deviations of the mean (but uses both the standard deviation of the data and the uncertainties given in Tables 5-8). It can be seen that for Case 1, both the uncertainty and standard deviations obey this rule as expected. It can be seen that for Cases 2-4, the differences are much larger, as previously discussed.

3.3. Selection of time interval

The sections above have focused their results on the time intervals 512, 1024, and 2048 μs. As shown in Table 2, time intervals down to 4 μs (for Cases 1 and 3) and 16 μs (for Cases 2 and 4) were performed. In order to determine which time interval(s) should be used in analysis, there are several considerations. The first is to understand how the uncertainty of each parameter varies as a function of the time interval. Figure 6 shows how the uncertainties in R_1 and Y_2 vary as a function of the time interval for Case 1. It is not surprising that the shape of the uncertainty in R_1 is very similar to the value of Y_2 (as seen in Figure 3).

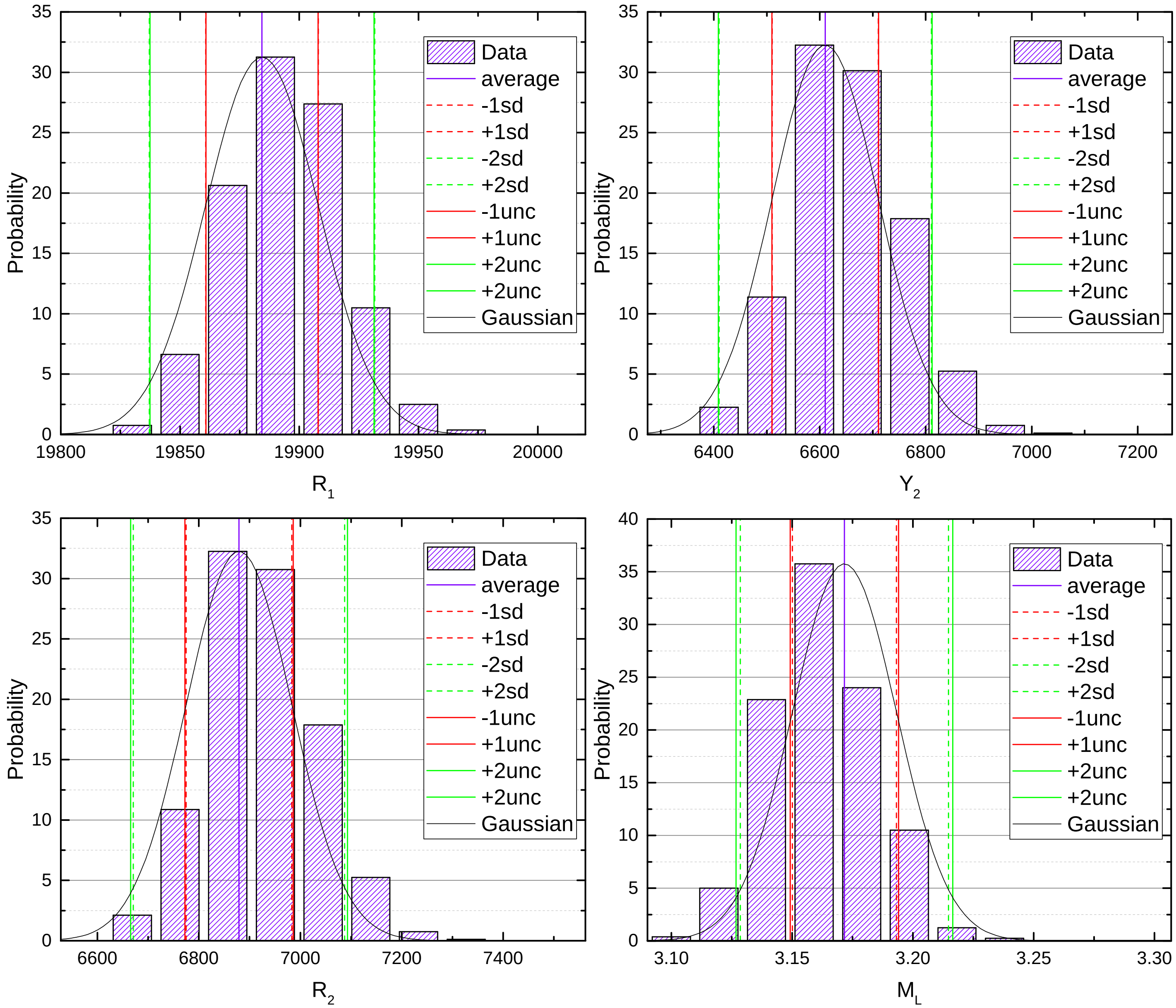

Figure 4: Histogram results using a time interval of 1024 μs for Case 1.

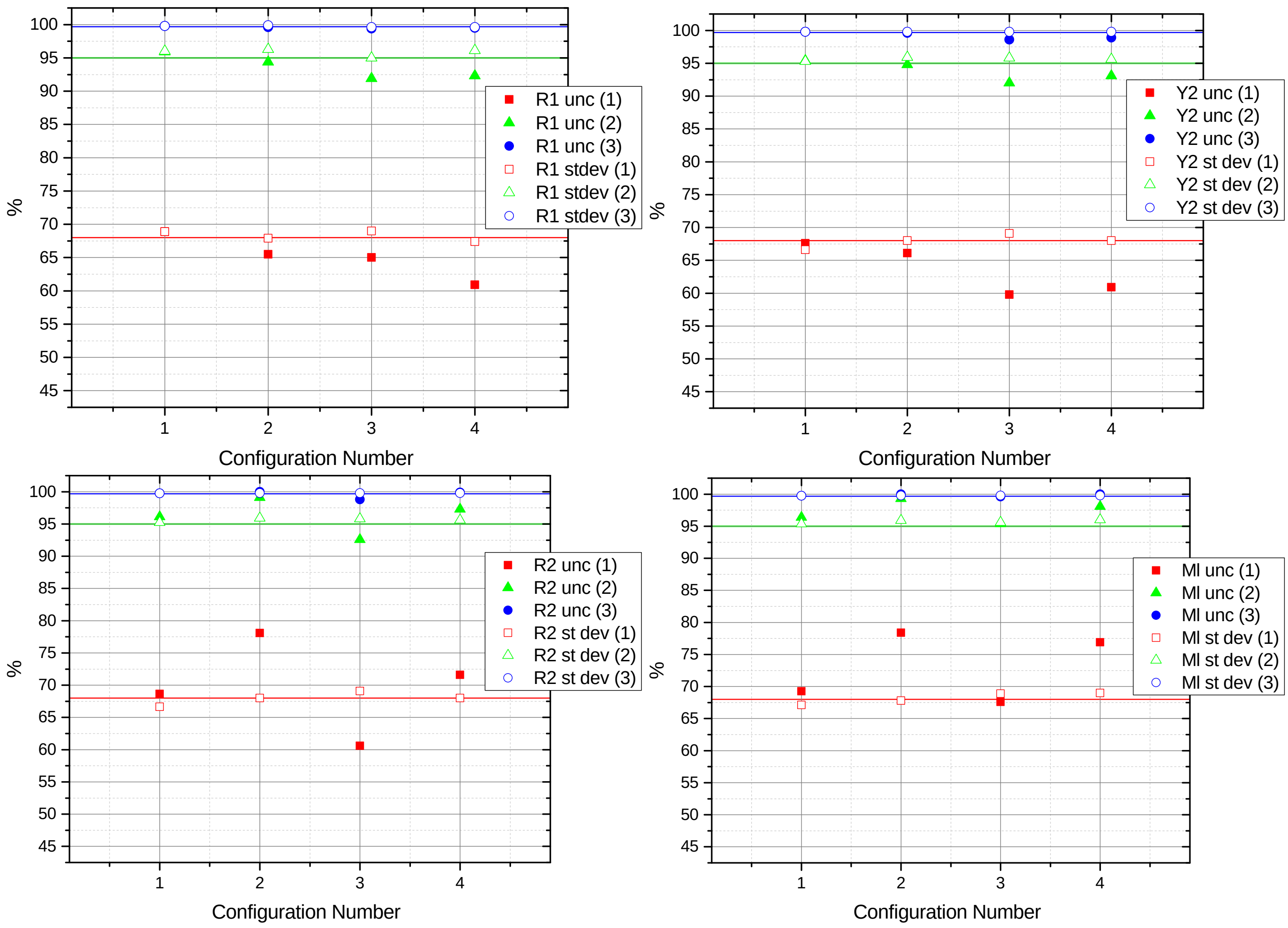

Figure 5: Percentage of data within 1, 2, or 3 σ at a 1024 μs time interval.

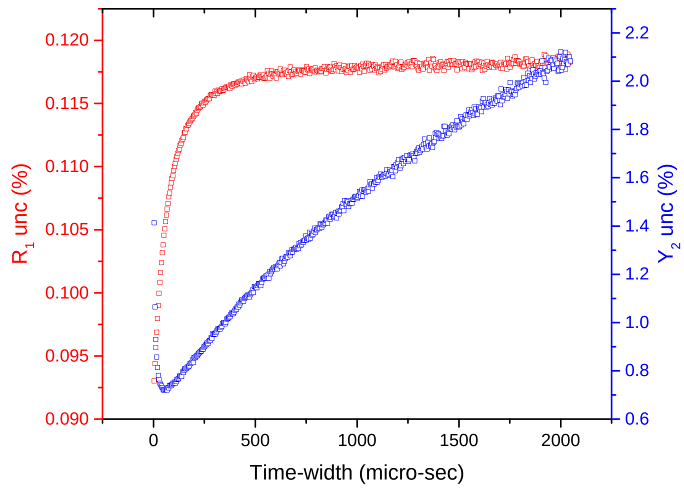

Figure 6: R_1 and Y_2 uncertainty versus time interval for Case 1 (file 1 of 800).

The similarities between the uncertainty in R_1 and the value of Y_2 can be seen by comparing Equations 28 and 18. The uncertainty in Y_2 is more complicated, but mostly increases (nearly linearly) as the time interval increases.

The uncertainties in R_2 and M_L are much more interesting. As shown in Equation 36, there are two parameters which contribute to the uncertainty in R_2: the uncertainty in Y_2 and the uncertainty in the neutron lifetime ($\frac{1}{\lambda}$). Figure 7 shows the uncertainty of R_2 as a function of the time interval for Case 1. This figure includes curves corresponding to different uncertainties in the neutron lifetime. As stated in Section 3.2.1, the uncertainty used for this parameter was bounding based upon multiple files and is the focus of future work. The shapes of curves in this figure includes two competing sets of parameters: one competition is between the uncertainty of the lifetime term versus the uncertainty in the Y_2 term and the other competition is between the uncertainty in Y_2 and the value of ω_2 (both are seen in Equation 29). It should be noted that the shapes of these curves can be quite different than those in Figure 7, but the main conclusions are always the same. If the uncertainty in the neutron lifetime is small, then the time interval that gives the smallest uncertainty in R_2 is small (often $< 100\ \mu s$). But as the uncertainty in the neutron lifetime increases, the time interval that

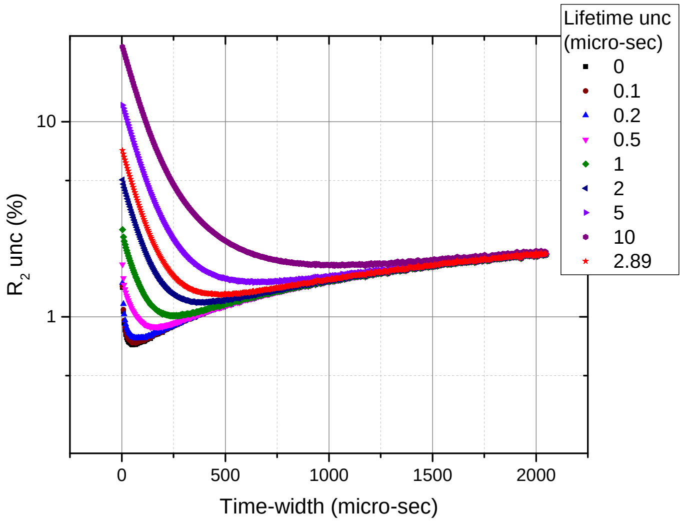

Figure 7: R_2 uncertainty versus time interval for Case 1 (file 1 of 800).

minimizes the uncertainty in R_2 also increases. If one does not have confidence in the uncertainty in the neutron lifetime, it is best to use a large time interval (it can be seen in Equation 32 that the value of the prompt neutron decay constant does not matter once the time interval approaches infinity). The red curve in Figure 7 corresponds to the uncertainty in the neutron lifetime used for Case 1 (2.89 μs). The shape of the uncertainty of leakage multiplication as a function of the time interval is not plotted because it is identical to the shape of the R_2 uncertainty. This is because the uncertainty in R_2 is much larger than the uncertainty in R_1 and therefore dominates the uncertainty in M_L (when the uncertainty in the efficiency is assumed to be zero).

As stated above, the optimal gate width really depends upon how large the uncertainty of the neutron lifetime is. So in reality the optimal gate width will vary for each configuration. It is sometimes useful, however, to use a single time interval when comparing results between different configurations. It is the opinion of the authors, that based on Figure 7 and similar figures for other systems, that a time interval between 1000-2000 μs is generally a sufficient compromise. This is because the uncertainty in R_2 is almost flat and the curves mostly overlap in this region.

3.4. Covariance between R_1 and R_2

As discussed in Section 2.6, and particularly in discussion of the equation which was used to determine the uncertainty in leakage multiplication (Equation 55), the covariance between R_1 and R_2 was assumed to be zero for this work. At this time, an analytical expression for this covariance has not been developed, but one can calculate the sample covariance of multiple files using Equation 16. This was done for the 800 files of Case 1, which resulted in a sample covariance of 459. Figure 8 shows how R_1 and R_2 are correlated (the slope of this graph is related to the sample covariance). When compared to the average square of the R_2 uncertainty the covariance is negligible ($\delta R_2^2 = 11409$). Including the covariance resulted in reducing the uncertainty in leakage multiplication for a single file from 0.0226 (with the assumed $\delta R_1 R_2 = 0$) to 0.0223 (with $\delta R_1 R_2 = 459$). Note that the uncertainty in leakage multiplication decreases when including this positive covariance because $\frac{\partial M_L}{\partial R_1}$ is negative and $\frac{\partial M_L}{\partial R_2}$ is positive (so multiplying them together gives a negative value, which reduces the uncertainties). The signs of these partial derivatives might seem incorrect when one looks at Equation 55, but the coefficient a_3 is negative (and the coefficient a_4 is positive), which flips the signs in these equations. Since including the covariance would only result in a very small reduction in the uncertainty of leakage multiplication, the covariance is negligible and the assumption used in Section 2.6 is valid.

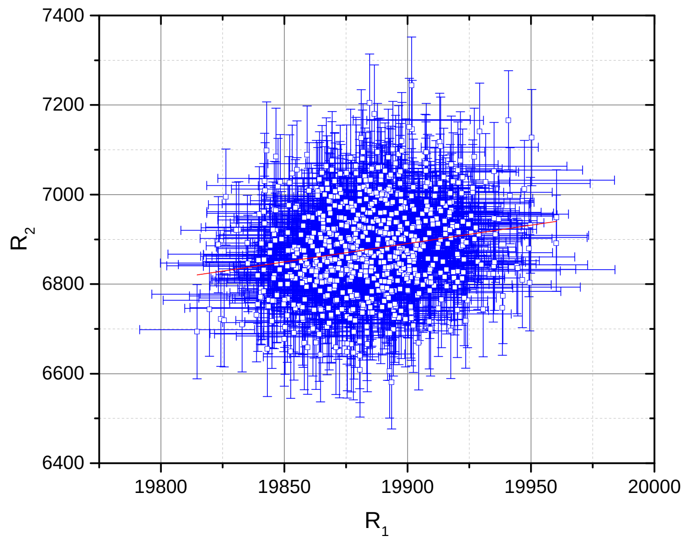

Figure 8: Covariance between $R_1$and $R_2$for Case 1 with a time interval of 1024 μs.

4. Conclusions

The Hage-Cifarelli formalism of the Feynman Variance-to-Mean method was presented and discussed. The uncertainties in six parameters were presented: singles count rate (R_1), Y_2, neutron lifetime ($\frac{1}{\lambda}$), doubles count rate (R_2), leakage multiplication (M_L), and spontaneous fission rate (F_S). A validation was then performed using data generated with a 0-D point-kinetics Monte Carlo code. This validation included four test cases, which varied in multiplication (values of 4.4 and 20 for total multiplication) and system lifetime (values of 40 and 200 μs). For each case, 800 files were generated (each with over 1 million events). For Case 1 (M_T = 4.4 and $\frac{1}{\lambda}$ = 40μs), the uncertainty method presented in this work agreed very well with the standard deviation of the data. For the other three cases, the agreement between the uncertainty method and the standard deviation of the data was not as good. This was due to violation of assumptions in the Hage-Cifarelli formalism (Cases 2 and 4) and/or extremely high count rates which resulted in large variations and uncertainties in some of the parameters (Cases 3 and 4). These three cases were meant to bound the types of data that would be recorded for most measurements in nuclear nonproliferation, safeguards, and criticality safety. So while Cases 2-4 do not agree as well, the fact that there is any agreement should make one conclude that the method presented is valid for most systems measured for these applications. Other users should, of course, ensure that their data are not outside the test cases studied (or better yet perform their own validation). Last, a discussion on the selection of time intervals for use with the Hage-Cifarelli formalism was presented. In Part II of this work, the same method and validation approach will be applied to recently measured subcritical benchmark data.

5. Acknowledgments

This work was supported by the Department of Energy Nuclear Criticality Safety Program, funded and managed by the National Nuclear Security Administration for the Department of Energy.

References

[1] *International Handbook of Evaluated Criticality Safety Benchmark Experiments* / Nuclear Energy Agency. - Paris : OECD Nuclear Energy Agency. 2016. (NEA;7328). 1, 2.8

[2] R. Bahran and J. Hutchinson. Subcritical copper-reflected α-phase plutonium (SCRαP) integral experiment design. *Transactions of the American Nuclear Society*, 114:527–529, 2016. 1

[3] B. Richard and J. Hutchinson. Tungsten-reflected plutonium-metal-sphere subcritical measurements. *In: International Handbook of Evaluated Criticality Safety Benchmark Experiments*, [DVD]/Nuclear Energy Agency. - Paris : OECD Nuclear Energy Agency, 2016. (NEA;7328). 1, 3.1

[4] B. Richard and J. Hutchinson. Nickel reflected plutonium metal sphere subcritical measurements. *In: International Handbook of Evaluated Crit-*

icality Safety Benchmark Experiments, [DVD]/Nuclear Energy Agency. - Paris : OECD Nuclear Energy Agency, 2016. (NEA;7328). 1, 3.1

[5] D.M. Cifarelli and W. Hage. Models for a three-parameter analysis of neutron signal correlation measurements for fissile material assay. *Nuclear Instruments and Methods in Physics Research Section A: Accelerators, Spectrometers, Detectors and Associated Equipment*, 251(3):550 – 563, 1986. 1, 2, 2.2, 2.3, 2.6

[6] J. A. Arthur, R. M. Bahran, J. D. Hutchinson, M. E. Rising, and S. A. Pozzi. Comparison of the performance of various correlated fission multiplicity monte carlo codes. *Transactions of the American Nuclear Society Winter Meeting and Technology Expo, 2016*, 2016. 1

[7] R. Bahran, J. Hutchinson, B. Richard, and A. Sood. List-mode simulations of the Thor core benchmark sensitivity experiments. *Transactions of the American Nuclear Society Annual Meeting*, 111:805–808, 2014. 1

[8] A. Sood, C. J. Solomon, J. D. Hutchinson, and R. Bahran. A review of recent R&D efforts in sub-critical multiplication measurements and simulations. *Transactions of the American Nuclear Society Annual Meeting, 2014*, 2014. 1

[9] S. R. Bolding and C. J. Solomon. Simulations of multiplicity distributions with perturbations to nuclear data. *Transactions of the American Nuclear Society*, 109:251–254, 2013. 1

[10] E. C. Miller, J. K. Mattingly, B. D. Dennis, S. D. Clarke, and S. A. Pozzi. Simulations of neutron multiplicity measurements with MCNP-PoliMi. *Technical Report SAND2010-6830, Sandia National Laboratories*, 2010. 1

[11] J. Mattingly. Polyethylene-reflected plutonium metal sphere: Subcritical neutron and gamma measurements. *Sandia National Laboratories Report SAND2009-5804*, 2009. 1

[12] J. Hutchinson, B. Mustafa, M. A. Smith-Nelson, W.L. Myers, T. E. Cutler, C. J. Solomon, A. Sood, D. R. Dinwiddie, and T. J. Grove. Subcritical multiplication experiments & simulations: Overview and recent advances. *Advances in Nuclear Nonproliferation Technology and Policy Conference 2016*, 2016. 1

[13] J. Hutchinson, B. Rooney, W. Myers, A. Sood, and M. Smith-Nelson. CALIBAN measurements near delayed critical using subcritical measurement methods. *American Nuclear Society Winter Meeting, Washington DC*, 2013. 1

[14] J. Hutchinson, M. A. Smith-Nelson, A. Sood, J. M. Goda, and J. A. Bounds. Joint LANL/CEA measurements on Godiva IV. *2014 American Nuclear Society Annual Meeting, Reno NV*, 2014. 1

[15] J. Hutchinson, A. Sood, W. Myers, M. Smith-Nelson, and D. Dinwiddie. Comparison of HEU measurements using measured and simulated data. *Transactions of the American Nuclear Society*, 106:487–489, 2013. 1

[16] J. Hutchinson, M. A. Nelson, A. Sood, D. K. Hayes, and R. G. Sanchez. Neutron noise measurements on HEU foils moderated by Lucite. *2015 American Nuclear Society Annual Meeting, San Antonio TX*, 2015. 1

[17] J. D. Hutchinson, M. A. Smith-Nelson, T. E. Cutler, B. L. Richard, and T. J. Grove. Estimation of uncertainties for subcritical benchmark measurements. *International Conference on Nuclear Criticality 2015*, 2015. 1, 2, 2.3, 3.1

[18] J. Hutchinson, B. Richard, M. Nelson, T. Grove, and T. Cutler. Uncertainty analysis of subcritical benchmark experiments using the Hage-Cifarelli formalism. *Internal report*, LA-UR-16-20375, 2016. 1, 2, 2.3, 3.1

[19] M. Nelson, T. Burr, J. Hutchinson, and T. Cutler. Uncertainties of the yn parameters of the Hage-Cifarelli formalism. *Los Alamos National Laboratory*, LA-UR-15-21365, 2015. 1, 2, 2.3, 2.3

[20] R. Uhrig. *Random Noise Techniques in Nuclear Reactor Systems.* The Ronald Press Company, 1970. 2, 2.5

[21] D. Cacuci. *Handbook of Nuclear Engineering.* Springer Science + Business Media LLC, 2010. 2

[22] R.P. Feynman, F. De Hoffmann, and R. Serber. Dispersion of the neutron emission in U-235 fission. *Journal of Nuclear Energy (1954)*, 3(1):64 – IN10, 1956. 2, 2.5

[23] T. Burr and K. Butterfield. Variance results for the second and third reduced sample moments in neutron multiplicity counting for randomly triggered or signal-triggered counting gates. *Nuclear Instruments and Methods in Physics Research Section A: Accelerators, Spectrometers, Detectors and Associated Equipment*, 594(2):257 – 265, 2008. 2, 2.3

[24] J. Verbeke. Determination of the standard deviation on multiplication based on count distributions. *Lawrence Livermore National Laboratory*, LLNL-TR-448118, 2010. 2, 2.3

[25] T. Burr and M. Nelson. Experimental verification of variance results for the second and third reduced factorial sample moments in neutron multiplicity counting. *International Journal of Recent Research and Applied Studies*, 13(2):353–357, 2012. 2

[26] Dina Chernikova, Kare Axell, Senada Avdic, Imre Pazsit, Anders Nordlund, and Stefan Allard. The neutron-gamma feynman variance to mean approach: gamma detection and total neutron-gamma detection (theory and practice). *Nuclear Instruments and Methods in Physics Research Section A: Accelerators, Spectrometers, Detectors and Associated Equipment*, 782(Supplement C):47 – 55, 2015. 2

[27] T. Cutler, M. Nelson, and J. Hutchinson. Deciphering the binning method uncertainty in neutron multiplicity measurements. *Transactions of the American Nuclear Society Winter Meeting*, 2014. 2.1

[28] A.A. Robba, E.J. Dowdy, and H.F. Atwater. Neutron multiplication measurements using moments of the neutron counting distribution. *Nuclear Instruments and Methods in Physics Research*, 215(3):473 – 479, 1983. 2.2

[29] G. Hansen. The rossi alpha method. *Los Alamos National Laboratory*, LA-UR-85-4176, 1985. 2.5

[30] J. Hutchinson, G. McKenzie, J. Arthur, M. Nelson, and W. Monange. Prompt neutron decay constant fitting using the rossi-alpha and feynman variance-to-mean methods. *Transactions of the American Nuclear Society Winter Meeting*, 117(1):986–989, 2017. 2.5, 3.2.1

[31] D. Reilly, N. Ensslin, and H. Smith. *Passive Nondestructive Assay of Nuclear Materials*. National Technical Information Service, 1991. 2.6

[32] Norman E. Holden and Martin S. Zucker. Prompt neutron emission multiplicity distribution and average values (nubar) at 2200 m/s for the fissile nuclides. *Nuclear Science and Engineering*, 98(2):174–181, 1988. 2.6

[33] J. Lestone. Energy and isotope dependence of neutron multiplicity distributions. *Los Alamos National Laboratory*, LA-UR-05-0288, 2005. 2.6, 3.1

[34] P. Santi and M. Miller. Reevaluation of prompt neutron emission multiplicity distributions for spontaneous fission. *Nuclear Science and Engineering*, 160(2):190–199, 2008. 2.6, 3.1

[35] J. Hutchinson, T. Cutler, T. Grove, and M. Nelson. A study of measured, experimental, and nuclear data uncertainties for subcritical benchmark experiments. *M&C 2017 - International Conference on Mathematics & Computational Methods Applied to Nuclear Science & Engineering*, 2017. 2.6

[36] J. Hutchinson, T. Grove, and M. Nelson. Uncertainty as a function of time for subcritical experiment parameters using the Hage-Cifarelli formalism. *Transactions of the American Nuclear Society Annual Meeting*, 2016. 2.6

[37] V. Dean and L. Blackwood. ICSBEP guide to the expression of uncertainties. *International Handbook of Evaluated Criticality Safety Benchmark Experiments*, NEA/NSC/DOC/(95)03/I, 2007. 2.8, 2.8, 3.2.1

[38] M. Nelson. Neutron generator: version 2.04. *LANL Software*, 2016. 3.1